

This is the accepted manuscript made available via CHORUS. The article has been published as:

## Parity of specular Andreev reflection under a mirror operation in a zigzag graphene ribbon

Yanxia Xing, Jian Wang, and Qing-feng Sun

Phys. Rev. B **83**, 205418 — Published 19 May 2011

DOI: [10.1103/PhysRevB.83.205418](https://doi.org/10.1103/PhysRevB.83.205418)

# The parity of specular Andreev reflection under mirror operation in zigzag graphene ribbon

Yanxia Xing<sup>1,3</sup>, Jian Wang<sup>1,\*</sup>, and Qing-feng Sun<sup>2,†</sup>

<sup>1</sup>*Department of Physics and the Center of Theoretical and Computational Physics,  
The University of Hong Kong,  
Pokfulam Road, Hong Kong, China.*

<sup>2</sup>*Beijing National Lab for Condensed Matter Physics and Institute of Physics,  
Chinese Academy of Sciences, Beijing 100080, China.*

<sup>3</sup>*Department of Physics,  
Beijing Institute of Technology, Beijing 100081, China.*

It is known that the parity of reflection amplitude can either be even or odd under the mirror operation. Up to now, all the parities of reflection amplitude in the one-mode energy region are even under the mirror operation. In this paper, we give an example of odd parity for Andreev reflection (AR) in a three-terminal graphene-superconductor hybrid systems. We found that the parity is even for the Andreev retroreflection (ARR) and odd for specular Andreev reflection (SAR). We attribute this remarkable phenomenon to the distinct topology of the band structure of graphene and the specular Andreev reflection involving two energy bands with different parity symmetry. As a result of odd parity of SAR, the SAR probability of a four-terminal system with two superconducting leads (two reflection interfaces) can be zero even when the system is asymmetric due to the quantum interference of two ARs.

PACS numbers: 72.80.Vp, 74.45.+c, 73.40.-c, 74.25.F-

## I. INTRODUCTION

Since the experimental realization of graphene<sup>1</sup>, it has become an exciting arena for theoretical and technological investigations.<sup>2</sup> A number of new phenomena have been predicted and verified experimentally. For instance, in the presence of magnetic field, it exhibits a distinctive half-integer quantum Hall effect.<sup>1</sup> Its quasi-particles obey the Dirac-like equation and have relativistic-like behaviors.<sup>2</sup> Due to the relativistic effect, the Klein tunneling occurs where an incident electron in graphene can pass through a potential barrier with probability one,<sup>3</sup> which induces the focusing of electron flow in a graphene p-n junction.<sup>4,5</sup> Besides, the well-separated valleys in zigzag edged nanoribbon can lead to the valley valve effect.<sup>6</sup>

Since good contacts between superconducting leads and graphene have been realized experimentally,<sup>7</sup> the transport study through graphene based normal-metal-superconductor (GNS) heterojunction becomes feasible. In the presence of a normal metal (graphene)-superconducting interface, an incoming electron converts into a hole and a cooper pair is formed that enters the superconductor. Due to the relativistic nature of the electron in graphene, the electron-hole conversion can either be intraband (within conduction or valence band) or interband (between conduction and valence bands). When the electron-hole conversion is intraband, it corresponds to the usual Andreev reflection (AR)<sup>8</sup> or Andreev retroreflection (ARR) because the reflected hole is along the incident direction. This ARR occurs for both relativistic and non-relativistic electrons. When the electron-hole conversion is interband, the reflected hole is along specular direction and a specular Andreev reflection (SAR) takes place,<sup>9</sup> which can lead to novel phenomena as we will discuss below.

It is known that the parity is a fundamental quantity in physics and reflection is a general physical phenomenon in

nature. In this paper, we discuss the parity of reflection amplitude for graphene in contact with superconductor leads. In general, the parity of a reflection amplitude can be either even or odd when the system is under mirror operation. However, for all previous known reflection events, the reflection amplitudes in the one-mode energy region have even parity under the mirror operation. It is yet to find an odd-parity reflection event. In this paper, we found, for the first time, that the SAR amplitude has an odd parity under the mirror operation for zigzag graphene ribbons with even number of chains. This means that the phases of SAR amplitude for a graphene-superconductor hybrid system and its mirror system differ by  $\pi$ . We attribute this phenomenon to the unique band structure of the graphene. Obviously this phase difference does not affect any observable quantities for each system. When two systems couple together, however, this  $\pi$  phase manifest through quantum interference between two SARs. So this  $\pi$  phase shift has important consequences for a four terminal device with two superconducting leads (see Fig.2(a)). When two superconducting leads are symmetrically attached to the device, the quantum interference of the left and right SAR leads to a destructive or constructive interference depending on whether the phase difference of superconducting leads is zero or  $\pi$ . Importantly, when two superconducting leads are *asymmetrically* attached to the device, the same interference pattern occurs provided that the Dirac point  $E_0$  is in line with the condensate of superconducting lead. The quantum interference between pairs of the AR can be tuned by shifting the Dirac point, the asymmetry of the two superconducting leads, as well as the phase between two superconducting leads. Due to the odd parity of SAR, the interference pattern for SAR is phase contrasted to that of ARR where the parity is even.

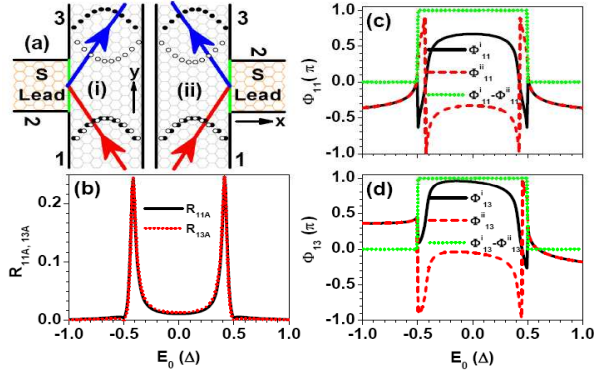


FIG. 1: (Color online) Panel (a): zigzag ribbons with even number of chains (gray honeycomb) attached by a superconducting lead on the left and right (orange honeycomb), respectively. For SAR the incoming electrons (red arrow) are scattered by the GNS junction (green solid line) as holes (blue arrow). The corresponding wave functions at sublattice “A” (solid circle) and “B” (hollow circle) for the lowest subband in conduction band (bottom) and the highest subband in valence band (top) are shown schematically. Panel (b): AR probability from terminal-1 to terminal-1  $R_{11A}$  and to terminal-3  $R_{13A}$  vs. Dirac point  $E_0$ . Panels (c) and (d): AR phase  $\Phi_{11}^{(i)}$  (c) and  $\Phi_{13}^{(ii)}$  (d) of two systems in panel (a) and their phase different  $\Phi_{11(13)}^{(i)} - \Phi_{11(13)}^{(ii)}$  vs.  $E_0$ .

## II. THEORY AND NUMERICAL RESULTS

Before doing numerical calculation, we first prove that the phases of SAR amplitude of two systems (i) and (ii) in Fig.1(a) differ by  $\pi$ , i.e., the parity of SAR is odd under mirror operation. Note that for graphene systems electrons in valence and conduction band are usually referred as electrons and holes, respectively. In the presence of superconducting lead the reference point of electrons and holes is the Fermi level in the superconducting lead. In the following, we will refer electrons (holes) as electrons above (below) Fermi level in superconducting lead. Denote  $\psi_c^+$  ( $\psi_v^+$ ) the wavefunction of electrons in conduction (valence) band moving in +y direction and  $\psi_c^-$  ( $\psi_v^-$ ) in -y direction in the zigzag graphene nanoribbon lead. It was known that under reflection  $\hat{P} : x \rightarrow -x$ ,  $\psi_c^\pm$  is symmetric while  $\psi_v^\pm$  is anti-symmetric if the energy of electron is in the first transmission channel<sup>10</sup>[see Fig.1(a)], i.e.,

$$\begin{aligned} \hat{P}\psi_c^\pm(x, y) &= \psi_c^\pm(-x, y) \\ \hat{P}\psi_v^\pm(x, y) &= -\psi_v^\pm(-x, y). \end{aligned} \quad (1)$$

which is one of the unique features of zigzag edge nanoribbons with even number of chains. Assuming the incident electron from the terminal-1, the wavefunctions for SAR  $\psi_{1,3}$  in zigzag nanoribbon lead 1 or 3 of the system (i) can be written as

$$\begin{aligned} \psi_1^{(i)} &= \psi_e^+ + r_{11}\psi_e^- + r_{11A}\psi_h^- \\ \psi_3^{(i)} &= t_{13}\psi_e^+ + r_{13A}\psi_h^+ \end{aligned} \quad (2)$$

where  $r_{11}$  is the normal reflection amplitude,  $t_{13}$  is the transmission amplitude,  $r_{11A}$  and  $r_{13A}$  are the Andreev reflection

amplitudes with the reflected hole to the terminal-1 and 3, respectively. Similarly the wavefunctions for the system (ii) are given by

$$\begin{aligned} \psi_1^{(ii)} &= \psi_e^+ + \bar{r}_{11}\psi_e^- + \bar{r}_{11A}\psi_h^- \\ \psi_3^{(ii)} &= \bar{t}_{13}\psi_e^+ + \bar{r}_{13A}\psi_h^+ \end{aligned} \quad (3)$$

Since the system (i) is related to (ii) by the reflection operator  $\hat{P}$ , we have  $\psi_\alpha^{(i)} = \hat{P}\psi_\alpha^{(ii)}$  with  $\alpha = 1, 3$ . Note that for SAR, the electron is in the conduction band while the hole is in the valence band, i.e.,  $\psi_e = \psi_c$  and  $\psi_h = \psi_v$ . From this relation together with Eqs.(1), (2), and (3), we obtain

$$\begin{aligned} r_{11A} &= -\bar{r}_{11A}, \quad r_{13A} = -\bar{r}_{13A} \\ r_{11} &= \bar{r}_{11}, \quad t_{13} = \bar{t}_{13} \end{aligned} \quad (4)$$

Note that the origin of this  $\pi$  phase shift (odd parity) is the interband conversion from the electron to the hole. Therefore the  $\pi$  phase shift does not occur for ARR since it involves only intraband conversion. Now we verify this statement numerically using a tight-binding model (see below for detailed description of the model and numerical procedure). The numerical results of AR probability  $R_{11A(13A)} = |r_{11A(13A)}|^2$  for two systems are shown in Fig.1(b). As expected the AR probability are exactly the same for two systems. However, the phase of AR amplitudes  $r_{11A(13A)}$  denoted as  $\Phi_{11(13)}^{i,ii}$  are different. It is shown in Fig.1(c) and Fig.1(d) that ARR amplitudes ( $|E_0| > |E_F|$ , with  $|E_F| = 0.5$ ) are the same for two systems in Fig.1(a) while the SAR amplitudes ( $|E_0| < |E_F|$ ) have a  $\pi$  phase shift. It confirms the odd parity for interband electron-hole conversion, which comes from the distinct topology of the band structure of graphene.

To see the consequence of the odd parity of SAR, we examine a symmetric four-terminal device with two superconducting leads depicted in Fig.2(a) (by setting asymmetry  $\delta N = 0$  and phase difference  $\delta\phi = 0$ ). For this system, two beams from terminal-1 has a  $\pi$  phase shift due to odd parity of SAR and interferes destructively at terminal-3 giving rise to a vanishing SAR coefficient. However, we can arrive the same conclusion using symmetry argument as follows. Since the system is symmetric with respect to  $x = 0$ , we must have  $r_{13A} = \bar{r}_{13A}$  when the reflection operation along x-direction is applied. While from Eq.(4),  $r_{13A} = -\bar{r}_{13A}$ . So the AR probability  $R_{13A} = |r_{13A}|^2$  for SAR can also be zero from symmetry point of view.<sup>11</sup> Therefore we conclude that the symmetric device can not be used to test the odd parity of SAR. In the following, we demonstrate that due to the  $\pi$  phase shift the destructive interference still occurs in a four-probe devices with two superconducting leads attached asymmetrically and hence can be used to test the odd parity of SAR.

For this purpose, we consider an asymmetric four-terminal device consisting of a zigzag graphene ribbon with two superconducting leads as shown in Fig.2(a). The Hamiltonian of the graphene is<sup>12</sup>  $H_0 = \sum_i \epsilon_i a_i^\dagger a_i - \sum_{\langle ij \rangle} t a_i^\dagger a_j$ . Here  $a_i$  and  $a_i^\dagger$  are the annihilation and creation operators at site  $i$ ,  $\epsilon_i$  is the on-site energy which can be controlled experimentally by the gate voltage<sup>1</sup>, and the hopping constant  $t = 2.75\text{eV}$  represents the nearest carbon bond energy. The pair potential (energy gap)

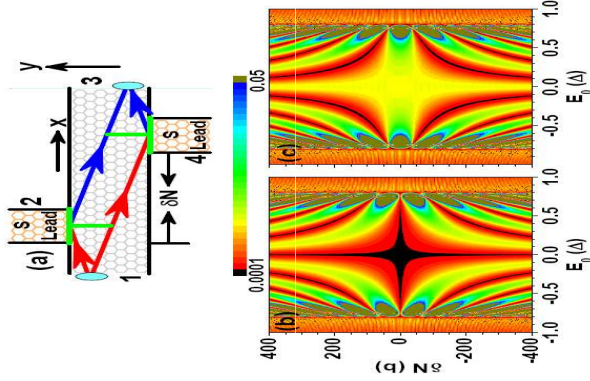


FIG. 2: (Color online) Panel (a): sketch of AR interferometer in which the zigzag ribbon is asymmetrically attached by two superconductor lead-2 and 4. Electrons in terminal-1 can be Andreev reflected into terminal-3 by either top or bottom GNS junction (horizontal green lines). Panel (b) and (c): the contour plot of  $R_{13A}$  vs Dirac point  $E_0$  and asymmetry  $\delta N$ . The phase difference of two superconductor leads  $\delta\varphi$  is zero in panel (b) and  $\pi$  in panel (c). The other parameters: Fermi energy  $E_F = 0.8$ , number of chains in zigzag ribbon  $N = 40$  corresponding to width  $60a$ , the width of superconductor lead  $W_S = 10b$ , where  $b = \sqrt{3}a$ .

of superconducting terminal- $\beta$  with  $\beta = 2, 4$  is  $\tilde{\Delta}_\beta = \Delta_\beta e^{i\varphi_\beta}$  with  $\Delta_2 = \Delta_4 = \Delta \simeq 1meV$ . In numerical calculations,<sup>11</sup> we fix Fermi energy  $E_F$  and tune the Dirac point  $E_0$ . We have used  $\Delta$  as the energy unit.

Now we study the interference between two ARs from GNS junctions as shown in Fig.2(a) in which two superconducting leads 2 and 4 are asymmetrically attached to the zigzag nanoribbon. The horizontal distance  $\delta N$  between two GNS junctions measures the asymmetry of two GNS junctions. The scattering process can be qualitatively understood as follows. For simplicity, we assume  $\phi_2 = \phi_4$  for the moment. As shown schematically in Fig.2(a), for SAR the particle-like electrons in terminal-1 split into two beams and are scattered separately by two GNS junctions (green horizontal lines) as holes that finally recombine at terminal-3. We examine the total phase accumulated for each beam that involves the following three processes. Before reaching the first GNS junction (denoted by the left vertical green line) two beams of electrons propagate with the same momentum  $k_x$ . After reaching the second GNS junction (denoted by the right vertical green line) two beams of holes also propagate with the same momentum  $k'_x$ . Obviously phases accumulated in the above two processes for both beams are the same. Between them two beams propagate with different momenta  $k_x$  and  $k'_x$ . Hence the phase difference between two beams is  $\phi = (k_x - k'_x)\delta x$  with  $\delta x = b\delta N$ , where  $b = \sqrt{3}a$  and  $a$  the lattice constant. This phase difference can be tuned by varying the Dirac point  $E_0$  or the asymmetry  $\delta N$  giving rise to a complicated interference pattern (see Fig.2). In particular, this phase difference can be zero if  $(k_x - k'_x) = 0$

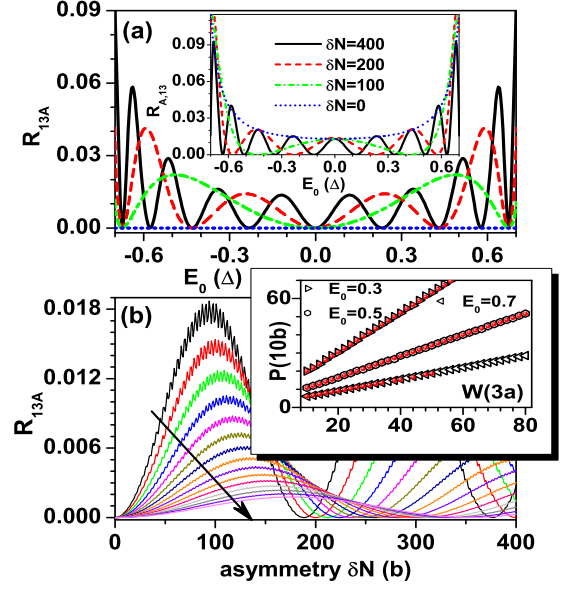


FIG. 3: (Color online) Panel (a): With fixed Fermi level  $E_F = 0.8$ , total AR probability  $R_{13A}$  vs Dirac point  $E_0$  for different asymmetry  $\delta N$ . In the main panel  $\delta\varphi = 0$ , and while  $\delta\varphi = \pi$  in the inset. Panel (b):  $R_{13A}$  vs asymmetry  $\delta N$  with  $E_0 = 0.3t$  for different width  $W$  from  $10 \times 3a$  to  $38 \times 3a$  with the interval  $2 \times 3a$  along the black arrow. Inset panel: the hollow signs are the period  $P$  obtained from the main panel and the solid red circles are the period  $P$  from the energy band with the expression  $P = 2\pi/(k_x - k'_x)$ . The other parameters:  $\delta\varphi = 0$ ,  $E_F = 0.8$ .

(i.e.,  $E_0 = 0$ ) or  $\delta N = 0$ . In general, the total phase difference is  $\phi = (k_x - k'_x)\delta x + \phi_2 - \phi_4$ .

Interference pattern of AR probability  $R_{13A}$  for system depicted in Fig.2(a) with pair potential phase difference of two superconductors  $\delta\varphi = 0$  and  $\pi$  ( $\delta\varphi \equiv \varphi_2 - \varphi_4$ ) are then plotted in Fig.2(b) and (c), respectively. For Fig.2(b) following observations are in order: (1) For the geometrically symmetric system ( $\delta N = 0$ ), the interference is always destructive with zero  $R_{13A}$  as long as  $|E_0| < |E_F|$ .<sup>11</sup> Clearly this is due to the  $\pi$  phase shift depicted in Fig.1(d) and is consistent with the band selection rule.<sup>10</sup> (2) When Dirac point  $E_0$  is in line with the condensate energy of the superconductor, i.e., when  $E_0 = 0$ ,  $R_{13A}$  is again zero no matter what value  $\delta N$  assumes. This means that there is a completely destructive interference between two beams scattered by two GNS junctions attached asymmetrically to the graphene nano-ribbon. This behavior can be understood as follows. When  $E_0 = 0$  the incoming electron and reflected hole have the same propagating momentum  $k_x$  and thus path 1 and 2 in Fig.2(a) experience the same quantum phase  $k_x\delta x$  except at the superconducting leads. Hence the total phase difference is only due to the  $\pi$  phase shift between two SARs. (3)  $R_{13A}$  is an even function of Dirac point  $E_0$  because of the electron-hole symmetry in graphene. Due to the geometric symmetry,  $R_{13A}$  is also an even function of asymmetry  $\delta N$ . (4) For nonzero  $E_F$ , the closer the Dirac point  $E_0$  to  $E_F$ , the more rapidly  $R_{13A}$  oscillates as we vary  $\delta N$ . This



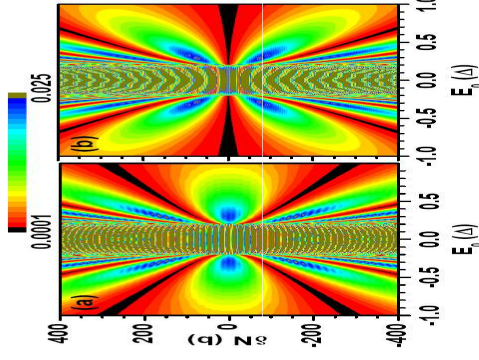


FIG. 4: (Color online) The interference pattern of AR from terminal-1 to terminal-1. The phase difference of two superconductor leads is zero in panel (a) and  $\pi$  in panel (b). The other parameters are same to Fig.2. except for  $E_F = 0.2$ .

is because the difference of propagating momentum  $k_x - k'_x$  increases monotonically as  $E_0$  approaches to  $E_F$ . (5) When  $E_0$  is in the vicinity of  $E_F$ ,  $R_{13A}$  can reach 0.9 which is much larger than that when  $|E_0| > |E_F|$ . This is because when  $E_F$  is very close to  $E_0$ , the edge states of zigzag ribbon begin to contribute, then electron is easier to be scattered by two GNS junctions located also at edges of zigzag ribbon. Considering the pseudo-spin conservation, large  $R_{13A}$  is always found in the region of  $|E_0| < |E_F|$ , i.e., the SAR region. (6) There is an overall fine oscillation with a period of  $\delta N = 3b$ . Similar behavior was also found in zigzag ribbons with a p-n junction where the conductance is determined by the relative displacement  $\delta$  along the p-n junction.<sup>13</sup> In Fig.2(c) with the superconducting phase difference  $\delta\phi = \pi$ , we see that the interference pattern is contrary to  $\delta\phi = 0$  [Fig.2(b)] where the constructive interference becomes destructive and vice versa.

To further analyze the interference pattern, we plot in Fig.3(a) the total  $R_{13A}$  vs Dirac point  $E_0$  for different asymmetry  $\delta N$  with the phase difference between two superconducting leads  $\delta\phi = 0$  [main panel of Fig.3(a)] or  $\delta\phi = \pi$  [inset of Fig.3(a)]. Clearly the interference (oscillatory) pattern occurs only for asymmetric systems ( $\delta N \neq 0$ ) with oscillation frequency proportional to  $\delta N$ . When pair potential phase difference  $\delta\phi = \pi$  is introduced, the interference pattern reverses, and  $R_{13A}$  with  $\delta N = 0$  becomes the envelop function of  $R_{13A}$  for all nonzero  $\delta N$ . In Fig.3(b) we plot  $R_{13A}$  vs  $\delta N$  for different widths  $W$  of nanoribbon. It is shown clearly that  $R_{13A}$  is a periodic function of  $\delta N$  with larger periodicity for larger  $W$ . In the inset of Fig.3(b) we plot this period versus the width for different  $E_0$ . The period  $P$  is obtained in two ways: (1). from the expression  $P = 2\pi/(k_x - k'_x)$  where the momenta  $k_x$  and  $k'_x$  can be obtained from the band structure for a given  $E_0$  (black symbols). (2). directly from main panel of Fig.3(b) (red solid circle). From the inset, it clearly shows that two periods are exactly the same giving strong evidence that the interference pattern of AR probability are indeed from two reflected hole beams.

Finally, the interference pattern of AR probability  $R_{11A}$  is

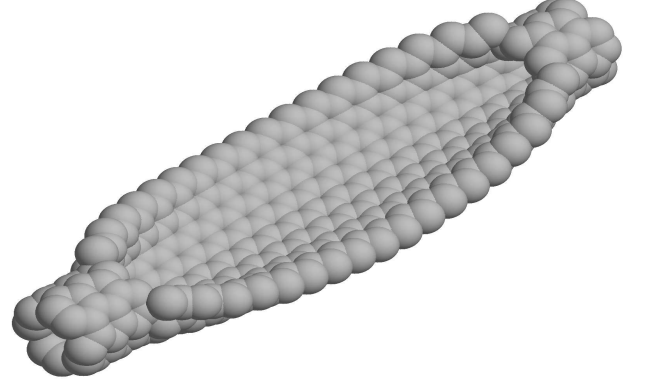


FIG. 5: (Color online) The schematic plot of partially unzipped CNT.

also studied (Fig.4). We found that only ARR probability  $R_{11A}$  ( $|E_0| > E_F = 0.2\Delta$ ) exhibits interference pattern. We note that since there is no  $\pi$  phase shift involved in ARR, when  $\delta N = 0$  reflected electrons through two GNS junctions interfere constructively when  $\delta\phi = 0$  and destructively when  $\delta\phi = \pi$  which is in contrast to SAR in Fig.2. In fact, interference patterns of SAR and ARR are always phase contrast not only for  $\delta N = 0$  but also for all other  $\delta N$ .

To test the odd parity of SAR experimentally, it relies on the fabrication of high quality zigzag graphene nanoribbons. It has been achieved by several laboratories using different methods last year including the method to unzip the carbon nanotube (CNT),<sup>14</sup> the anisotropic etching by thermally activated nickel nanoparticles,<sup>15</sup> and use chemical method<sup>16</sup> and reconstruction of the edge<sup>17</sup> to make zigzag graphene nanoribbons. In view of the above experimental breakthrough, we expect that the setup to test our predicted phenomenon can be realized experimentally.

To reduce the experimental challenge, we have considered an unzipped CNT device, i.e., (n,n) CNT-zigzag graphene-(n,n) CNT, obtained by unzipping a few unit cells in the central part of an armchair CNT which has been achieved experimentally (see Fig.5).<sup>14</sup> For this system, the wavefunction in the armchair CNT has the same symmetry as that of the zigzag graphene ribbon. Following the same procedure leading to Eq.(4), we have shown that the unzipped CNT in contact with a superconducting lead has the odd parity under mirror operation. Similar conclusions drawn from GNS can be obtained for unzipped CNT with two superconducting leads.

### III. CONCLUSION

In conclusion, up to now, the parity of reflection amplitude was found to be even under the mirror operation. Here we have provided an example of odd parity for the reflection amplitude, the SAR amplitude in the zigzag graphene-superconductor hybrid system. This odd parity is due to the combination of unique band structure of the graphene and the electron-hole conversion involving two energy bands with different parity symmetry. The signature of odd parity of SAR

can be found from the quantum constructive interference in a four terminal system with two superconducting leads attached asymmetrically. Furthermore, the interference pattern due to odd parity of SAR is phase contrasted to that of ARR where the parity is even.

**Acknowledgement** We gratefully acknowledge the financial support from a RGC grant (HKU 705409P) from the

Government of HKSAR and from NSF-China under Grant Nos.10974236 and 10821403.

\*e-mail: jianwang@hkusua.hku.hk.

†e-mail: sunqf@aphy.iphy.ac.cn.

- 
- <sup>1</sup> K. S. Novoselov, A.K. Geim, S.V. Morozov, D. Jiang, Y. Zhang, S.V. Dubonos, I.V. Grigorieva, and A.A. Firsov, *Science* **306**, 666 (2004); K. S. Novoselov, A. K. Geim, S.V. Morozov, D. Jiang, M.I. Katsnelson, I.V. Grigorieva, S. V. Dubonos, and A.A. Firsov, *Nature (London)* **438**, 197 (2005); Y. Zhang, Y.-W. Tan, H.L. Stormer, and P. Kim, *Nature (London)* **438**, 201 (2005).
  - <sup>2</sup> C. W. J. Beenakker, *Rev. Mod. Phys.* **80**, 1337 (2008); A. H. Castro Neto, F. Guinea, N.M.R. Peres, K.S. Novselov, and A.K. Geim, *Rev. Mod. Phys.* **81**, 109 (2009).
  - <sup>3</sup> M. I. Katsnelson, K. S. Novoselov and A. K. Geim, *Nature Phys.* **2**, 620 (2006); A.-F. Young et al, *Nature Phys.* **5**, 222 (2009); Andrei V. Shytov, Mark S. Rudner, and Leonid S. Levitov, *Phys. Rev. Lett.* **101**, 156804 (2008).
  - <sup>4</sup> V. V. Cheianov et al, *Science* **315**, 1252 (2007).
  - <sup>5</sup> Y. Xing, J. Wang and Q.-F. Sun, *Phys. Rev. B* **81**, 165425 (2010).
  - <sup>6</sup> A. Rycerz, J. Tworzydło, and C. W. J. Beenakker, *Nature Phys.* **3**, 172 (2007).
  - <sup>7</sup> H. B. Heersche, P. Jarillo-Herrero, J. B. Oostinga, L. M. K. Vandersypen, and A. F. Morpurgo, *Nature* **446**, 56 (2007); F. Miao, S. Wijeratne, Y. Zhang, U.C. Coskun, W. Bao, and C.N. Lau, *Science* **317**, 1530 (2007).
  - <sup>8</sup> A. F. Andreev, *Sov. Phys. JETP* **19**, 1228 (1964).
  - <sup>9</sup> C. W. J. Beenakker, *Phys. Rev. Lett.* **97**, 067007 (2006).
  - <sup>10</sup> J. Nakabayashi, D. Yamamoto, and S. Kurihara, *Phys. Rev. Lett.* **102**, 066803 (2009).
  - <sup>11</sup> S. Cheng et al, *Phys. Rev. Lett.* **103**, 167003 (2009); Q.-F. Sun and X.C. Xie, *J. Phys.: Condens. Matter* **21**, 344204 (2009).
  - <sup>12</sup> D. N. Sheng, L. Sheng, and Z. Y. Weng, *Phys. Rev. B* **73**, 233406 (2006); Z. Qiao and J. Wang, *Nanotechnology* **18**, 435402 (2007). W. Long, Q.-F. Sun, and J. Wang, *Phys. Rev. Lett.* **101**, 166806 (2008); J. Li and S.-Q. Shen, *Phys. Rev. B* **78**, 205308 (2008).
  - <sup>13</sup> A. R. Akhmerov, J. H. Bardarson, A. Rycerz and C. W. J. Beenakker, *Phys. Rev. B* **77**, 205416 (2008).
  - <sup>14</sup> L. Jiao, L. Zhang, X. Wang, G. Diankov, H. Dai, *Nature (London)*, **458**, 877 (2009); D. V. Kosynkin, A. L. Higginbotham, A. Sinitskii, J. R. Lomeda, A. Dimiev, B. K. Price, and J. M. Tour, *ibid*, **458**, 872 (2009).
  - <sup>15</sup> L. C. Campos, V. R. Manfrinato, J. D. Sanchez-Yamagishi, J. Kong and P. Jarillo-Herrero, *Nano. Lett.* **9**, 2600 (2009).
  - <sup>16</sup> X. Li, X. Wang, L. Zhang, S. Lee, and H. J. Dai, *Science* **319**, 1229 (2008).
  - <sup>17</sup> X. Jia, M. Hofmann, V. Meunier, B. G. Sumpter, J. Campos-Delgado, J. M. Romo-Herrera, H. Son, Y.-P. Hsieh, A. Reina, J. Kong, M. Terrones, and M. S. Dresselhaus, *Science*, **323** 1701 (2009); Ç. Ö. Girit, J. C. Meyer, R. Erni, M. D. Rossell, C. Kisielowski, L. Yang, C.-H. Park, M. F. Crommie, M. L. Cohen, S. G. Louie, and A. Zettl, *ibid*, **323** 1705 (2009).